Pergamon

PII: S0042-6989(97)00278-2

Vision Res., Vol. 38, No. 9, pp. 1239–1251, 1998

Printed in Great Britain
0042-6989/98 $19.00 + 0.00

Spatial Uncertainty and Sampling Efficiency in Amblyopic Position Acuity

HONG WANG,* DENNIS M. LEVI,†‡ STANLEY A. KLEIN*

Received 21 March 1996; in revised form 4 April 1997; in final form 6 August 1997

Spatial uncertainty and undersampling are two of the major hypotheses for the losses of amblyopic spatial vision. To test these two hypotheses, equivalent spatial uncertainty and spatial integration efficiency in spatial position judgments were quantified with a spatial perturbation paradigm. Specifically, three-line bisection thresholds were measured for the amblyopic eyes of two strabismic and two anisometropic amblyopes, and for normal controls. The horizontal stimulus lines comprised discrete dark dots distributed randomly around the mean line position according to a gaussian function. Line separation, the number of dots on each line (N), stimulus contrast (C), and the vertical standard deviation (σ_e) of the dot distribution were varied. An ideal observer analysis quantified the magnitude of equivalent spatial uncertainty (σ_s), the effective number of dots used (k), and spatial integration efficiency (k/N). At the optimal separation, equivalent spatial uncertainty (σ_s) is approximately ten-fold higher in *both* types of amblyopic visual systems than in control observers, even when stimulus visibility is accounted for. This apparent increase in σ_s is largely due to a shift in spatial scale of analysis in the amblyopic eye. Integration efficiency (k/N) increases in proportion to stimulus contrast or visibility (in units of detection threshold). Unlike σ_s, k/N is different between the two types of amblyopia. For the *anisometropic* observers, k/N is quantitatively similar to that of control observers. For the *strabismic* observers, on the other hand, k/N is reduced even after taking stimulus visibility into account. The decreased spatial integration efficiency in the strabismic visual system suggests that spatial undersampling may occur at a secondary stage of visual processing, beyond the detection stage. © 1998 Elsevier Science Ltd. All rights reserved.

Amblyopia Bisection Uncertainty Undersampling Efficiency

INTRODUCTION

Spatial vision in amblyopia is severely degraded (for reviews see Hess, Field & Watt, 1990; Levi, 1991). The nature of this degradation is not yet fully understood. Two of the major hypotheses§ proposed in the literature are (i) spatial undersampling (e.g., decrease in neuronal spatial sampling density) (Levi & Klein, 1986, 1996; Levi, Klein & Yap, 1987; Wilson, 1991; Levi, Klein & Wang, 1994a,b); and (ii) spatial uncertainty (e.g., spatial scrambling and/or an upward shift in the scale of spatial filter sizes) (Levi & Klein, 1985; Watt & Hess, 1987; Wilson, 1991; Hess & Field, 1994). However, controversies exist regarding these two hypotheses, particularly as applied to strabismic amblyopia (see for example, Hess & Field, 1994; Levi & Klein, 1996).

One way to distinguish between these two hypotheses is to estimate both spatial uncertainty and sampling efficiency of the amblyopic visual system using a spatial perturbation paradigm. This approach has been widely used to understand the limits of normal spatial vision (e.g., Zeevi & Mangoubi, 1984; Watt, Ward & Casco, 1987 have measured spatial uncertainty, and Andrews, Butcher & Buckley, 1973; Watt & Andrews, 1982 and Morgan & Glennerster, 1991 have measured sampling efficiency). In amblyopes, several studies have shown increased spatial uncertainty in the amblyopic eye (e.g. Watt & Hess, 1987; Kiorpes, Kiper & Movshon, 1994). Other experiments suggest that strabismic amblyopes require more samples for optimal performance than normal eyes (Levi & Klein, 1986). However, to date, no single study has estimated *both* the spatial uncertainty and the sampling efficiency in amblyopic eyes. Because spatial uncertainty and sampling efficiency can trade off in their effects, it is critical to determine both in the same observers (Wang, Levi & Klein, 1996). In our study, we employed a three-line bisection task where the observers judged the position of the central line relative to the center of the two outer lines. Spatial perturbation was introduced independently into each outer line by decomposing the lines into discrete dark dots distributed

*University of California at Berkeley, School of Optometry, Berkeley, California, U.S.A.
†University of Houston, College of Optometry, Houston, Texas, U.S.A.
‡To whom all correspondence should be addressed.
§A third hypothesis, namely alterations in the size of cortical receptive fields (i.e., a change in the spatial scale of processing—Hess & Holliday, 1992; Levi, Waugh, & Beard, 1994c) is for the present subsumed under the two hypotheses listed above, and will be discussed further in the Discussion section.

randomly around the intended line position according to a gaussian function.

Assuming that (i) spatial uncertainty (σ_i, i.e., the equivalent intrinsic uncertainty, which is the standard deviation of the dot positions due to uncertainty in the internal representation) and stimulus spatial perturbation (σ_e, i.e., the standard deviation of the externally applied perturbation of the dot positions) are independent; (ii) only k dots are effectively used out of N dots comprising a line; and (iii) spatial uncertainty of the solid central comparison line is σ_c, then the bisection threshold (B_{th}) can be modeled as:

$$B_{th} = \sqrt{\frac{\sigma_e^2 + \sigma_i^2}{2k} + \sigma_c^2} \qquad (1)$$

according to the position averaging of an ideal observer (Wang *et al.*, 1996). By applying this model to the experimental data, one is able to estimate both spatial uncertainty (σ_i) and integration (or sampling) efficiency (k/N) for both amblyopic and normal visual systems. We call this quantity "efficiency" following Barlow (1962) and Pelli (1990). Importantly, the two hypotheses (scrambling and undersampling) make different predictions. If amblyopia is a consequence of increased spatial scrambling, sampling efficiency would not be reduced (i.e., increased σ_i, same k). On the other hand, if amblyopia is a consequence of undersampling, then sampling efficiency will be low and spatial uncertainty will be unchanged (i.e., decreased k, same σ_i).

According to our ideal averaging model [equation (1)], bisection threshold (B_{th}) should be hardly affected by spatial perturbations (σ_e) when σ_e is far less than the spatial uncertainty (σ_i). When σ_e becomes comparable with σ_i, B_{th} will be noticeably elevated. Further increase in σ_e will proportionally elevate B_{th}. At the very high end of σ_e, B_{th} will be mainly determined by σ_e and k (i.e., $B_{th} \approx \sigma_e/\sqrt{(2k)}$), and σ_i will hardly play any role. This behavior, predicted by an ideal observer model, has been observed in previous studies (Zeevi & Mangoubi, 1984; Hess *et al.*, 1990; Watt & Hess, 1987; Wang *et al.*, 1996). The solid curve in Fig. 1 represents the performance of the normal visual system based on the simplified model described in equation (2), in which σ_i and σ_c are combined (discussed in the Methods section). If only spatial uncertainty (σ_i) were elevated in amblyopic vision, then the amblyopic data should be predicted by the dashed curve (indicating an additive factor). If only sampling efficiency (k/N) were degraded, then the amblyopic data should be predicted by the dotted curve (indicating a multiplicative effect). If both hypotheses were correct, then the amblyopic data will be expected to follow the pattern depicted by the dot-dashed curve due to the effects of both additive and multiplicative factors. The thin solid 45 deg line in Fig. 1 represents the performance of an ideal observer with no spatial uncertainty ($\sigma_s = 0$) and 100% efficiency ($k = N$).

Using this spatial perturbation paradigm, we shall show that, relative to the normal visual system, there is approximately a ten-fold increase in spatial uncertainty in *both* anisometropic and strabismic visual systems, and more than a three-fold loss of integration efficiency, but only in the strabismic visual system. The increase in spatial uncertainty is largely attributed to a shift in the spatial scale of analysis in the amblyopic eye. The loss of integration efficiency is equivalent to spatial undersampling in the strabismic visual system.

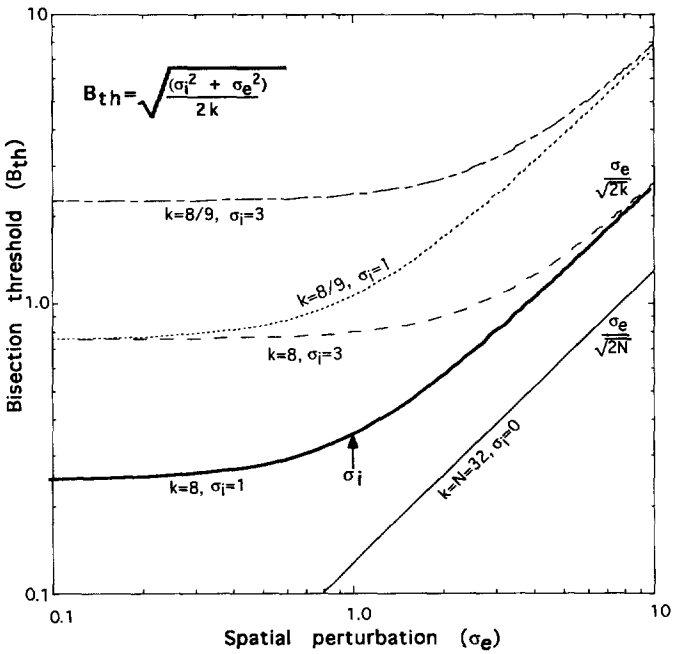

FIGURE 1. Bisection thresholds (B_{th}) predicted by our averaging model [equation (2)] are plotted against the magnitude of spatial perturbation (σ_e) on arbitrary logarithmic scales for various levels of spatial uncertainty (σ_s) and sampling efficiency (k/N). Suppose the data of a normal visual system is represented by the thick solid curve. Increased spatial uncertainty (an additive factor) is represented by the dashed curve. Decreased sampling efficiency (a multiplicative factor) is represented by the dotted curve. The combined effects of increased spatial uncertainty and decreased sampling efficiency are shown by the dot-dashed curve. The thin solid 45 deg line represents the performance of an ideal observer with no spatial uncertainty ($\sigma_s = 0$) and 100% efficiency ($k = N$). The height of this thin line is given by $B_{th} = \sigma_e/(2N)^{1/2}$.

METHODS

A detailed account of the experimental paradigm, stimuli and procedures can be found elsewhere (Wang *et al.*, 1996). The following is a general and supplementary description of the methods as applied to the present study.

The two outer lines of the three-line bisection stimuli comprised discrete dark dots whose positions were distributed around the intended line position according to a gaussian function (see Fig. 2). The central solid line was not perturbed, and had a fixed stimulus strength (C, in units of %min, i.e., Weber contrast times line width) to serve as a high-fidelity probe. The number of dots (N) displayed on each perturbed "line", the magnitude of spatial perturbation (σ_e, the standard deviation of the gaussian distribution) and stimulus strength were varied. Bisection thresholds were measured by judging the

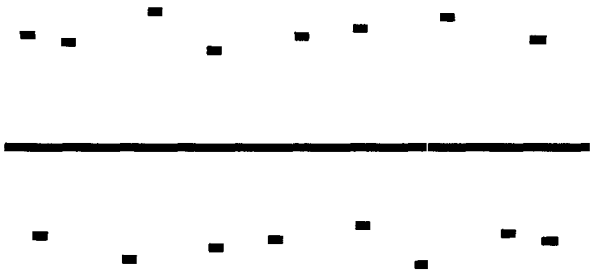

FIGURE 2. An example of a spatially perturbed stimulus for three-line bisection where the two outer lines comprise discrete dark dots.

position of the central line relative to the center of the two outside lines with a method of constant stimulus procedure, analyzed via a multi-rating ROC analysis (Levi, Klein & Aitsebaomo, 1984) and with threshold specified at $d' = 1$.

Two anisometropic (observers RM and BJ) and two strabismic (observers RH and AJ) amblyopes, all highly experienced psychophysical observers, participated. The visual characteristics of the four amblyopes are given in Table 1. Data were collected for both amblyopic and non-amblyopic eyes. Previously published data (Wang *et al.*, 1996) from three normal observers (HW, PY, and SW) are used as the controls.

To ensure comparable stimulus visibility for amblyopic observers, stimulus size was scaled up relative to that for normal observers, based on their relatively larger Ricco's diameter (see next paragraph). A dot size (length) of 1.36 min was used for the non-amblyopic eye, and 2.72 min for the amblyopic eye (compared with 0.68 min for control observers). In all cases, the full line (e.g., central line) consisted of 40 (non-resolvable) dots. In other words, the line length was 40 dots long.

To determine the visibility (in units of the detection threshold) of the scaled stimuli, detection thresholds were measured for sampled, unperturbed lines for each amblyopic observer. A single sampled line was displayed for 600 msec. The contrast of the line was randomly selected from four preset contrast levels, which included a zero contrast (blank) stimulus. The observer responded by pressing one of the four buttons corresponding to the perceived line contrast. The response was recorded by the computer, which gave auditory feedback about the true stimulus level of the previous trial and then displayed the next trial. Data were analyzed and detection thresholds were calculated using a multi-rating ROC method, as for bisection thresholds.

Detection thresholds were also measured for various line widths in order to estimate Ricco's diameter. Thus, for bisection stimuli, the line width could be strictly controlled to be less than Ricco's summation width. This enabled us to specify line strength meaningfully (as the product of line width and contrast; Klein, Casson & Carney, 1990). For simplicity, detailed data about detection thresholds at various line widths will not be presented in the Results section. We found that Ricco's line width is approx. 1 min for normal vision, and is increased to approx. 2 min for the amblyopic eyes (see also Levi & Klein, 1990; Levi *et al.*, 1994a).

In the first experiment, thresholds for three-line bisection without spatial sampling and perturbation (i.e., with solid and straight lines) were measured at various line separations. This first experiment served two purposes: (1) to determine the base performance without spatial perturbation; and (2) to determine the optimal line separation, where the bisection threshold is the lowest. By identifying the optimal line separation, we can isolate the most sensitive mechanisms for the subsequent perturbation experiments.

In the second experiment, spatial sampling and perturbation were introduced into the bisection task at the optimal line separation, such that equivalent uncertainty and integration efficiency can be determined. However, there is a problem in directly applying equation (1) for data modeling, since σ_i and σ_c are mathematically correlated in the equation and one of them becomes a redundant parameter for the purpose of curve fitting and modeling. To solve this dilemma, a simplified equation:

$$B_{\text{th}} = \sqrt{\frac{\sigma_e^2 + \sigma_s^2}{2k}} \qquad (2)$$

is used for parameter fitting, where σ_s can be regarded as an upper bound of spatial uncertainty σ_i. This simplifica-

TABLE 1. Visual characteristics of the amblyopic observers

Observer	Age	Sex	Eye	Rx.	Acuity*	Fixation†	Strabismus
Anisometropic‡							
RM	23	M	O.D.	− 2.00	20/15	Central	Occasional L. XT
			O.S.	− 12.50	20/70	Central	5–10$^{\Delta}$ when tired
BJ	27	M	O.D.	pl/ − 0.25 × 180	20/12	Central	None
			O.S.	+ 3.75/ − 1.50 × 20	20/52	Central	
Strabismic							
RH	23	M	O.D.	− 1.00/ − 0.50 × 170	20/15	Central	
			O.S.	− 1.50/ − 1.50 × 10	20/68	Unsteady	Microtropia L. ET, 2$^{\Delta}$
AJ	30	F	O.D.	+ 5.50/ − 2.50 × 20	20/60	1.5 deg Temporal	Constant R. XT, 4$^{\Delta}$
			O.S.	− 0.25	20/15	Central	

*75% Correct on Davidson–Eskridge charts.

†Fixation determined with Haidinger's brushes and visuoscopy.

‡No constant strabismus, and hyperopic anisometropia > + 1.5 D or myopic anisometropia > 4 D.

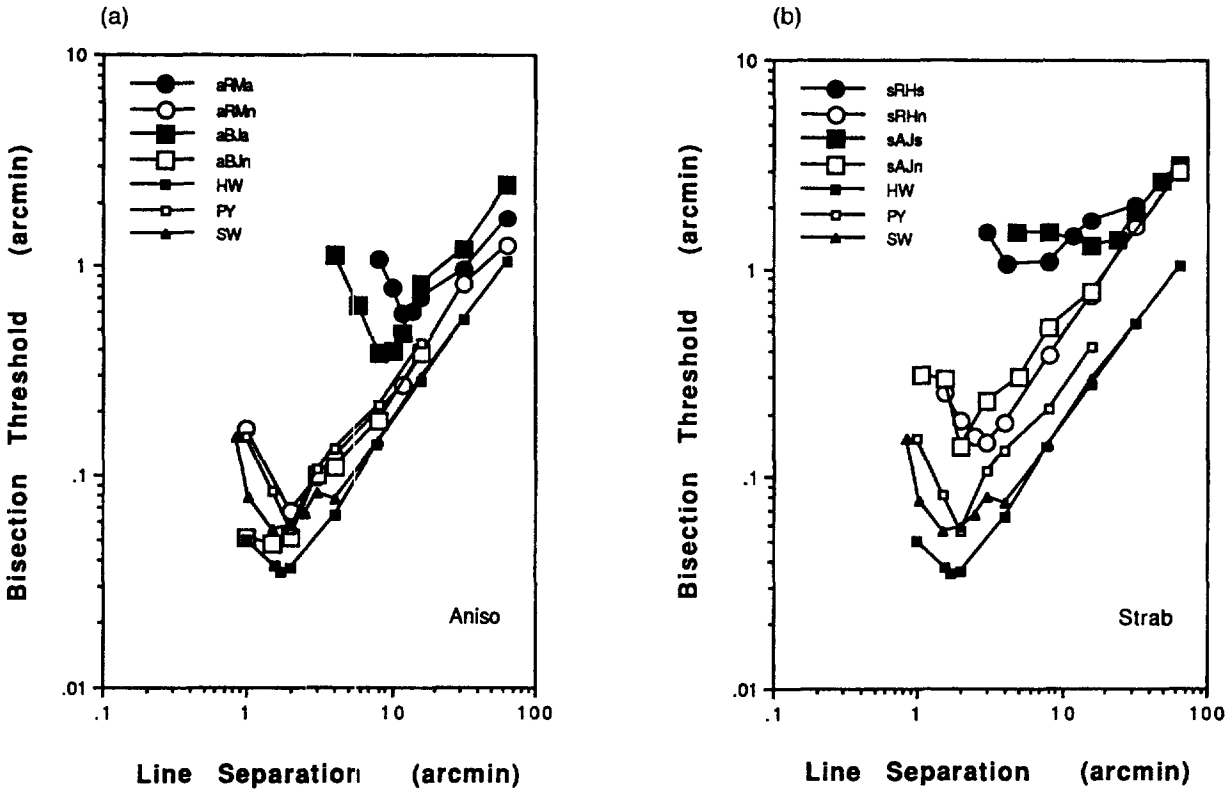

FIGURE 3. Bisection thresholds are plotted against line separation for anisometropic (a) and strabismic (b) observers. Large filled symbols are for the data of amblyopic eyes, and large open symbols are for the data of non-amblyopic eyes. Small symbols represent the data from the control observers.

tion should have little effect on our estimation of k, since k is mainly determined by the very high end of σ_e [i.e., $B_{th} \approx \sigma_e/\sqrt{(2k)}$].

Data fitting was accomplished using Igor^{TM} software, which uses the Levenberg–Marquardt algorithm to search for the parameter values that minimize chi-square.

RESULTS

Experiment 1. Bisection without spatial perturbation

To determine the optimal separation, bisection thresholds were measured at various line separations with three solid lines for each observer. Thresholds are plotted in Fig. 3 for both anisometropic [Fig. 3(a)] and strabismic [Fig. 3(b)] observers.

For anisometropic amblyopic eyes [large filled symbols in Fig. 3(a)], the data are located up and right relative to that of control observers (small symbols). Accordingly, the optimal separation is also shifted to a higher value of approx. 10 min arc. The closely similar shapes of the anisometropic and control data curves suggest that similar operations occur in each of these visual systems, but at different spatial scales, as indicated by the different optimal separations. For strabismic eyes [large filled symbols in Fig. 3(b)] however, thresholds at small separations are almost flat, with no obvious optimum. The lack of a clearly defined optimum may indicate a loss of the underlying normal mechanisms, or at least indicates that the mechanisms may be severely degraded.

There are at least two related reasons to focus our attention on the small or optimal separation regime. One is that the most sensitive mechanisms can be isolated for study, and the other is that the strabismic visual system is particularly degraded in this regime. Therefore, spatial uncertainty and integration efficiency were measured at the optimal line separations for both eyes of each observer in the next experiment. Note that the optimal separations were taken to be at 2 min for control eyes. For anisometropic eyes [Fig. 3(a)], we used 12 min for RM and 10 min for BJ. For strabismic eyes [Fig. 3(b)], the optimal separation is not well defined. For the purpose of this study, we selected a separation of 8 min for RH (large filled circles), and 10 min for AJ (large filled squares). Data were also obtained at larger separations, where the amblyopic deficit is much smaller, and these are all summarized in the lower portion of Table 2.

Experiment 2. Bisection with spatial perturbation

Bisection thresholds were measured at optimal and relatively wide line separations for each eye with varying contrast, number of samples, and magnitude of gaussian position jitter.

Some examples of the raw data from all amblyopic eyes at the optimal line separation are plotted in Fig. 4 (anisometropic amblyopes) and Fig. 5 (strabismic

TABLE 2. Stimulus and model parameters

Obs	Eye	Separ	N	C	V_l	V_d	Th_o	σ_s	k	k/N
aBJ	a	10	40	11	4.0	0.25	0.80	2.8	5.5	0.14
			40	19	5.9	0.37	0.55	2.2	8.2	0.20
			40	37	11.5	0.72	0.44	2.1	13.4	0.34
			40	56	17.4	1.09	0.32	1.7	16.4	0.41
aRM	a	12	40	80	3.8	0.60	0.73	3.6	12.0	0.30
			40	132	6.2	0.98	0.49	2.2	10.0	0.25
sAJ	s	10	16	112	2.9	0.72	1.21	1.1	0.4	0.03
			32	112	4.4	0.78	0.72	1.3	1.7	0.05
sRH	s	8	8	112	2.4	0.85	3.12	3.2	0.6	0.07
			16	112	3.2	0.80	1.63	2.2	1.0	0.06
			32	112	4.5	0.80	1.02	1.4	0.9	0.03
			32	56	2.3	0.41	1.44	0.9	1.8	0.03
aBJ	n	10	40	11	3.0	0.19	0.39	1.0	4.1	0.10
			40	18	4.9	0.31	0.31	1.5	13.2	0.33
			40	36	9.9	0.62	0.25	1.7	23.4	0.58
		2	40	18	4.9	0.31	0.29	1.1	5.9	0.15
			40	28	7.7	0.48	0.18	0.6	7.9	0.20
			40	56	15.3	0.96	0.05	0.4	21.9	0.55
	a	64	4	112	6.8	2.40	2.36	3.7	1.2	0.30
			8	112	10.4	2.19	2.10	4.2	2.1	0.26
			16	112	17.7	2.21	1.91	5.3	4.2	0.26
aRM	n	12	32	27	3.0	0.22	0.34	0.7	2.4	0.07
			32	45	5.0	0.37	0.27	0.9	5.7	0.18
		2	4	56	1.5	0.53	0.41	0.6	1.0	0.25
			8	56	2.5	0.53	0.27	0.5	1.9	0.24
			16	56	3.7	0.46	0.17	0.4	3.5	0.22
			32	56	6.2	0.46	0.07	0.3	12.0	0.38
	a	64	8	112	2.5	0.89	1.83	4.1	2.6	0.33
			16	112	3.0	0.75	1.44	5.1	5.6	0.35
			32	112	5.0	0.88	1.27	7.4	16.5	0.52
sAJ	n	2	16	56	3.2	0.40	0.32	0.7	2.9	0.18
			32	56	6.0	0.45	0.16	0.3	2.5	0.08
			32	28	3.0	0.22	0.32	0.6	1.7	0.05
		32	4	56	1.6	0.57	2.13	2.3	0.6	0.15
			32	56	6.0	0.45	0.75	2.2	4.8	0.15
	s	32	4	112	1.8	0.90	2.41	2.2	0.5	0.12
			32	112	4.4	0.78	1.31	2.8	2.4	0.07
			32	28	1.1	0.19	1.37	1.4	0.5	0.02
sRH	n	3	16	56	4.4	0.55	0.49	1.1	2.7	0.17
			32	56	7.7	0.57	0.32	0.7	2.4	0.07
		8	32	14	1.9	0.14	0.78	0.7	0.5	0.02
			32	28	3.8	0.28	0.51	1.0	2.1	0.07
			32	56	7.7	0.57	0.36	1.1	4.5	0.14
			8	56	3.2	0.67	0.73	1.4	1.9	0.24
			16	56	4.4	0.55	0.52	1.2	2.9	0.18
	s	32	4	112	1.9	0.95	4.46	4.8	0.6	0.15
			16	112	3.2	0.80	2.91	6.7	2.8	0.17
			32	112	4.5	0.80	1.95	6.7	5.5	0.17
			16	56	1.6	0.40	4.36	4.9	0.6	0.04

Obs, different observers, a for anisometropic, s for strabismic; Eye, eyes tested, a for anisometropic amblyopic eye, s for strabismic amblyopic eye, n for non amblyopic eye; Separ, the line separations used; N, number of dots; C, stimulus strength (in %min) of stimulus line; V_l, visibility of an undersampled line (in detection threshold units as will be presented in Fig. 9); V_d, the estimated visibility of a single dot in the context of a dotted line; Th_o, the measured bisection thresholds (in min) without external perturbation (i.e., $\sigma_e = 0$); σ_s, equivalent spatial uncertainty (in min); k, equivalent effective number of dots; k/N, equivalent integration efficiency. a, amblyopia; s, strabismus.

amblyopes). In each plot, bisection thresholds (B_{th} in min) are plotted against the magnitude of spatial perturbation (σ_e in min). Different symbols represent different combinations of stimulus parameters as listed in the figure legend, where C is the stimulus strength (in units of %min), N is the number of dots, and V_l is the stimulus visibility (in multiples of the detection threshold) of the undersampled "line". Data were fit by equation (2), and the curves are the results of the fit. Corresponding to each curve, the fit parameters (the effective number of dots, k, and spatial uncertainty, σ_s) are also listed in the plot legend. σ_s is in units of minutes, and corresponds to the horizontal knee position of each curve. k Is mainly determined by the thresholds at large values of spatial perturbation. Error bars in all the plots were omitted for clarity, and would be in the range of

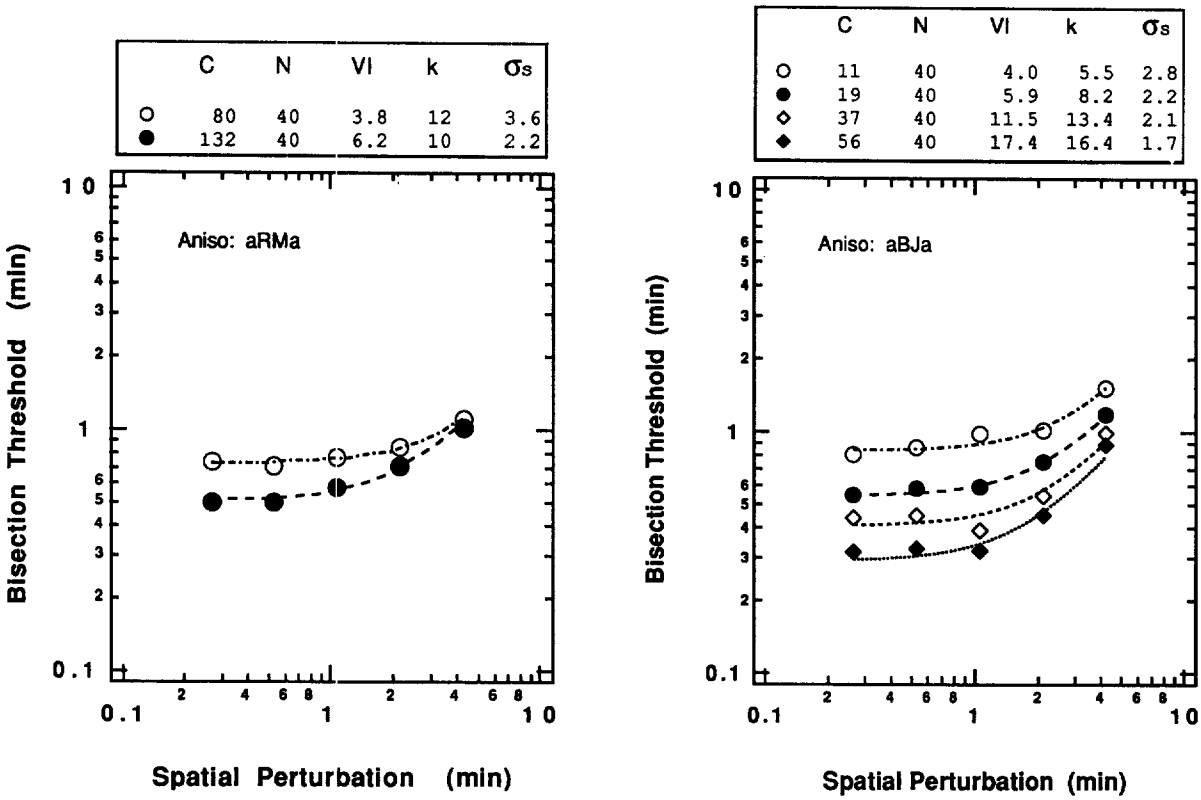

FIGURE 4. Bisection thresholds for the amblyopic eyes of two anisometropic observers, BJ (right) and RM (left), are plotted separately. In each plot, bisection thresholds are plotted against the magnitude of spatial perturbation. Different symbols represent the data for different combinations of the stimulus strength (C), numbers of dots (N), and visibility (V_l) of the sampled "line", as specified in the legend. Curves are fit to the data with equation (2), and the fit parameters (k and σ_s) are also listed in the plot legend.

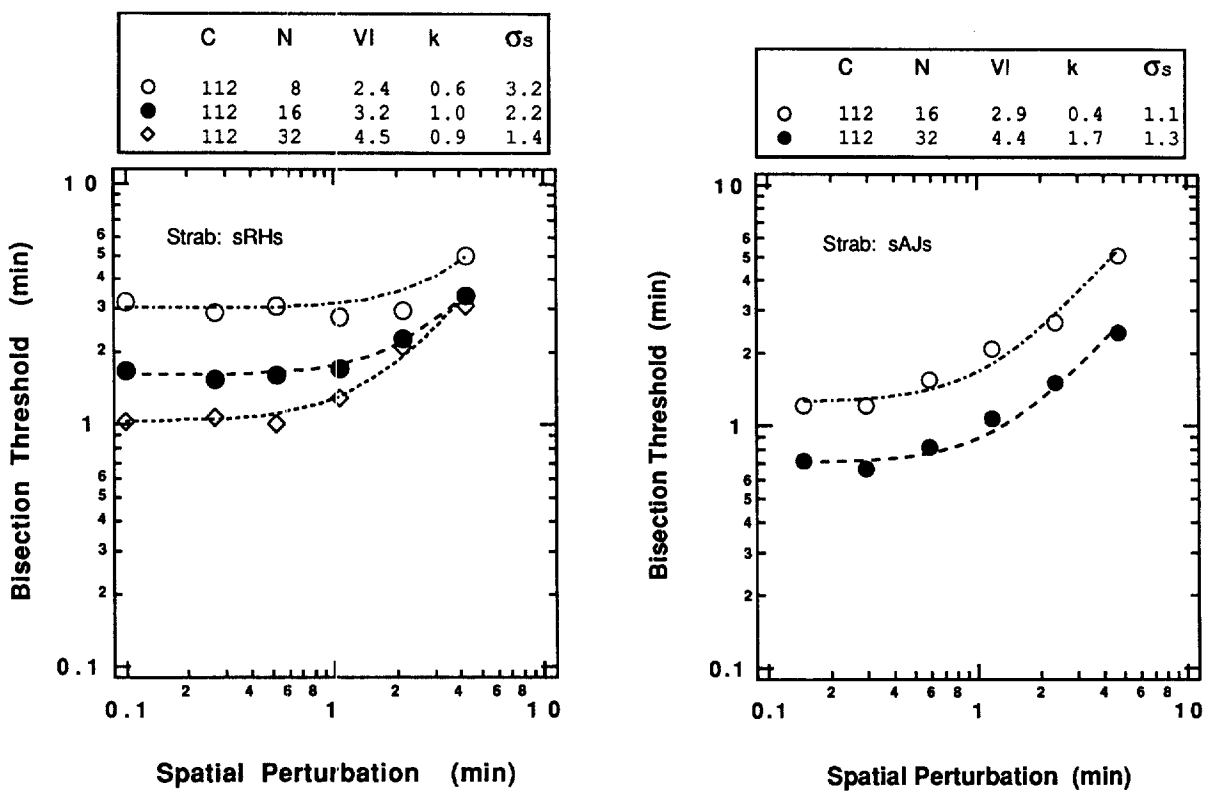

FIGURE 5. Bisection thresholds for the amblyopic eyes of two strabismic observers AJ (right) and RH (left) are plotted separately. See details in Fig. 4 legend.

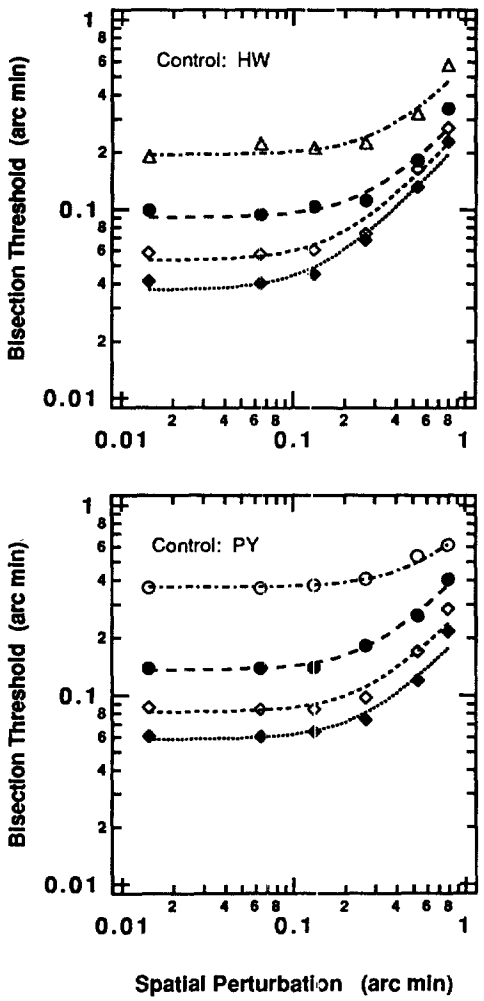

	C	N	Vl	k	σs
△	18	24	3.2	1.7	0.25
●	28	24	4.9	4.9	0.19
◇	42	24	7.4	6.6	0.13
◆	56	24	9.8	8.5	0.11

	C	N	Vl	k	σs
○	14	32	2.7	1.3	0.38
●	28	32	5.4	2.5	0.19
◇	42	32	8.2	6.2	0.18
◆	56	32	10.9	11.3	0.18

FIGURE 6. Bisection thresholds for two of the control observers HW (top) and PY (bottom) from a previous study (Wang *et al.*, 1996) are replotted here.

approx. 10% of the estimated parameter. For convenience of comparison, data for two of the control observers (HW and PY) from a previous study are also replotted in Fig. 6 (see Fig. 5 in Wang *et al.*, 1996).

As expected from the model [equation (2)], for a given combination of stimulus parameters, N and C, bisection thresholds are relatively unaffected by spatial perturbation (σ_e) up to a certain level, indicating the existence of an equivalent spatial uncertainty (σ_s). This behavior is evident across all the observers. However, quantitative differences do exist among the data of these visual systems. For similar stimulus conditions (e.g., similar line visibility, V_l), thresholds of the amblyopic eyes (Figs 4 and 5) are shifted up and to the right relative to that of controls (Fig. 6). According to our ideal averaging model (see Fig. 1), this quantitative difference between the thresholds of amblyopic eyes and control observers can now be described in terms of elevated spatial uncertainty (data curve shift up and right) and reduced sampling efficiency (data curve shift up) in all four amblyopic visual systems, as directly reflected in the two key parameters σ_s and k.

The two parameters (σ_s and k) derived for all the amblyopic observers are summarized in the top portion of Table 2 (for data displayed in Figs 4 and 5) along with a number of other important experimental parameters. Data from relatively wide separation bisection and from the normal fellow eye are also summarized in the lower portion of Table 2.

According to the model [equation (2)], the measured thresholds listed in the eighth column in Table 2 (Th_o) are very closely predicted by the two parameters listed in the ninth and tenth columns (σ_s and k). The prediction is: $Th_o = \sigma_s/\sqrt{(2k)}$. To get a more general picture, bisection thresholds (Th_o) along with the two key parameters (σ_s and k) will be plotted and analyzed. In the following figures, we show how the poor performance of bisection in amblyopia can be attributed to increased equivalent spatial uncertainty (σ_s) and decreased spatial sampling (k).

In Fig. 7, bisection thresholds without spatial perturbation (i.e., Th_o in the eighth column of Table 2) are plotted against line visibility (i.e., V_l in the sixth column of Table 2), where different symbols represent the data from different observers. The reason we choose line visibility as the independent variable for this figure is that line

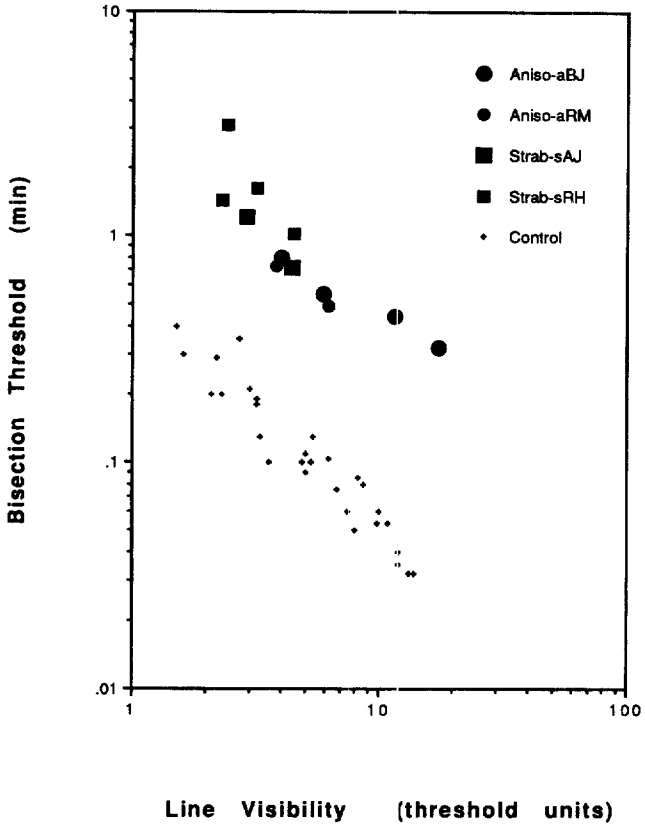

FIGURE 7. Bisection thresholds without spatial perturbation (i.e., Th_0 in the eighth column of Table 2) are plotted against line visibility (i.e., V_l in the sixth column of Table 2) in log–log coordinates. Data from different observers are plotted with different symbols. Filled circles are for the data of the amblyopic eyes of anisometropic observers, filled squares are for amblyopic eyes of strabismic observers, and smallest symbols are for that of control observers.

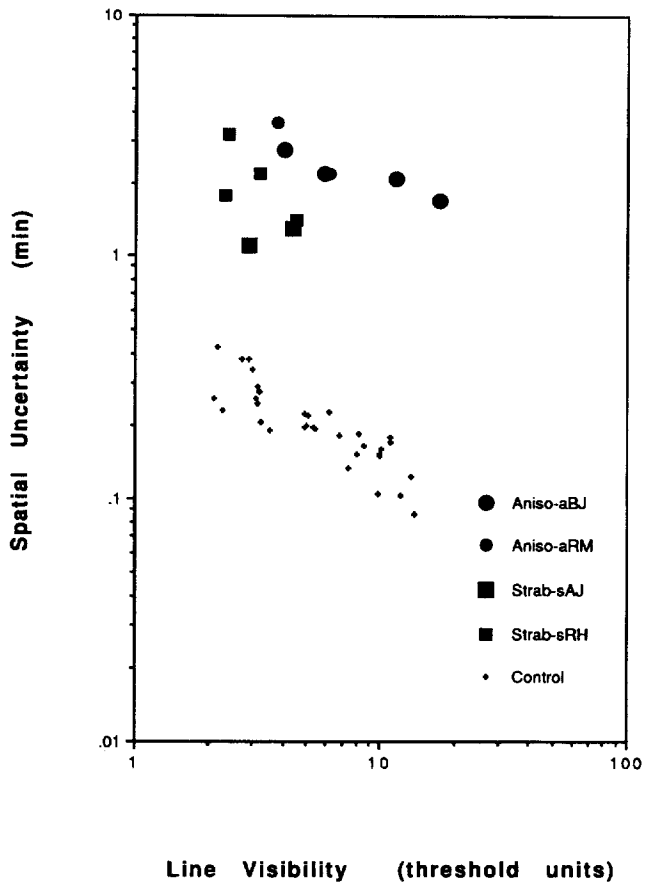

FIGURE 8. Spatial uncertainties (σ_s in the ninth column of Table 2) are plotted against line visibility (V_l in the sixth column of Table 2) for all the observers. The same symbols are used as in Fig. 7.

visibility is a critical factor in determining bisection threshold (Wang *et al.*, 1996). For all the observers, bisection threshold decreases as stimulus visibility increases following almost a reciprocal relationship, which indicates that a contrast-sensitive mechanism may be involved in bisection at the optimal separation in each of the visual systems under the study. However, there is almost a ten-fold loss of performance in the amblyopic visual systems (large filled symbols) relative to that of controls (small symbols from previous study in Wang *et al.*, 1996) at the same visibility level.

Figure 8 shows the relationship between spatial uncertainty (σ_s in the ninth column of Table 2) and line visibility (V_l in the sixth column of Table 2) for different observers (different symbols). Spatial uncertainties in all the amblyopic eyes (large filled symbols) are about ten-fold higher than that of normal controls (small symbols), with the anisometropic eyes (filled circles) particularly elevated. Another interesting pattern shown in this plot is that spatial uncertainty is visibility dependent, most clearly seen in the normal and anisometropic observers. This pattern is not consistent with the notion of a fixed intrinsic positional uncertainty due to spatial scrambling. An additive model with increased intrinsic positional uncertainty due to spatial scrambling would result in an elevated threshold that is independent of stimulus visibility (Levi *et al.*, 1994a). This visibility dependent behavior does make sense in terms of contrast-sensitive filter mechanisms, where visibility is directly related to signal-to-noise ratio (Wang *et al.*, 1996).

To evaluate the loss of integration efficiency, an intuitive way is to plot integration efficiency (k/N in the last column of Table 2) against line visibility as we did in the previous two figures. However, this would be misleading, since line visibility is determined by both stimulus strength and the number of dots. Consider two lines with the same visibility (i.e., equal multiples above the line detection threshold), but one line has fewer dots and higher contrast than the other. The first line will certainly yield a higher integration efficiency than the second one, even though they have the same visibility.

A more plausible way to account for visibility is to consider the visibility of a single dot, rather than that of a line. A straightforward way to determine the visibility of a dot is by measuring the detection threshold of a single dot. However, the visibility of an isolated dot is not necessarily the same as that of a dot in the context of a dotted line. Furthermore we just cannot simply measure the detection threshold of a single dot owing to the limitations of the equipment and human vision, since the

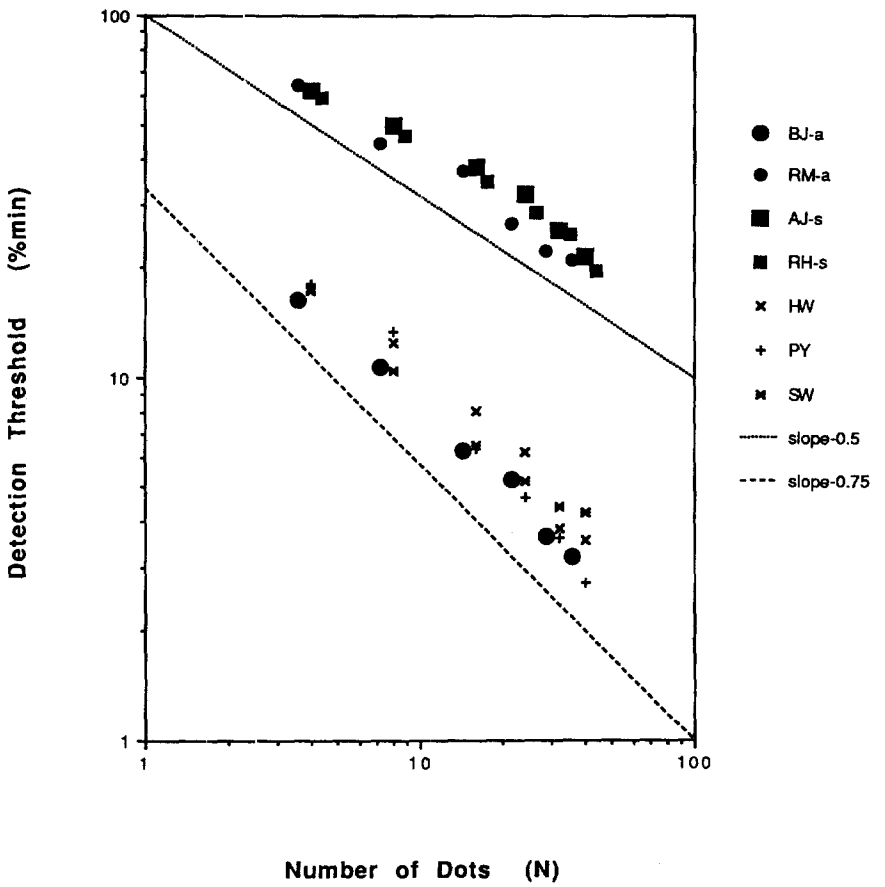

FIGURE 9. Line detection thresholds for all the amblyopic eyes are plotted against the number of dots comprising the line. Different symbols represent the data of different observers. Large filled symbols are for amblyopic eyes, and the other small symbols are for control observers. The two arbitrarily positioned lines indicate the slopes of −0.5 (dotted line) and −0.75 (dashed line). Note that the data of some observers are positioned with a relative horizontal offset of approx. 10% to avoid the overlap with the data of others. Otherwise, all the data should be on one of the horizontal positions of 4, 8, 16, 24, 32, and 40 dots.

visibility of a single dot was often less than 1, i.e., below detection threshold.

Thus, the visibility of a single dot (V_d) in the context of a perturbed line needs to be estimated for different stimulus conditions. V_d (as listed in the seventh column of Table 2) was estimated by extrapolating the line's visibility, V_l (as listed in the sixth column of Table 2) as a function of N (the number of dots on the line) to the visibility of a single dot ($N = 1$) with the following equation:

$$V_d = V_l N^{\text{Slope}}, \tag{3}$$

where Slope (a negative value) is determined from individual fits for each eye of each observer, to the data in Fig. 9.

In Fig. 9, line detection thresholds are plotted against the number of dots for all the observers. Large filled symbols are for amblyopic eyes, and the other symbols are for control observers. Detection thresholds of the amblyopic eyes (large filled symbols except that of BJ-a) are elevated, and follow a slope of approx. −0.5 (arbitrarily positioned dotted line). Detection thresholds of anisometropic observer BJ-a (large filled circles) are about the same as that of control observers (HW, PY, and SW), which have a slope of approx. −0.75 (arbitrarily positioned dashed line). Of course the detection thresholds of the amblyopic observers would be much higher if dot size (length) had not been scaled.

Integration efficiency (k/N in the last column of Table 2) now can be plotted against dot visibility (V_d in the seventh column of Table 2) for different observers, as shown in Fig. 10. For anisometropic amblyopia (filled circles), integration efficiencies are almost the same as, or even slightly higher than, those of control observers (small symbols). Thus, spatial integration or sampling in the anisometropic visual system is essentially normal or even better. For strabismic amblyopia (filled squares), integration efficiencies are lower by almost a factor of ten relative to that of control observers (small symbols), indicating that spatial integration or sampling is truly degraded in the strabismic visual system.

The above data analysis focused on bisection at the optimal line separation where the most sensitive mechanisms are involved and are most severely degraded. For bisection at relatively wide line separations, data were also analyzed and are summarized in the lower portion of Table 2 along with the data from the fellow normal eye. The main findings from wide line separations

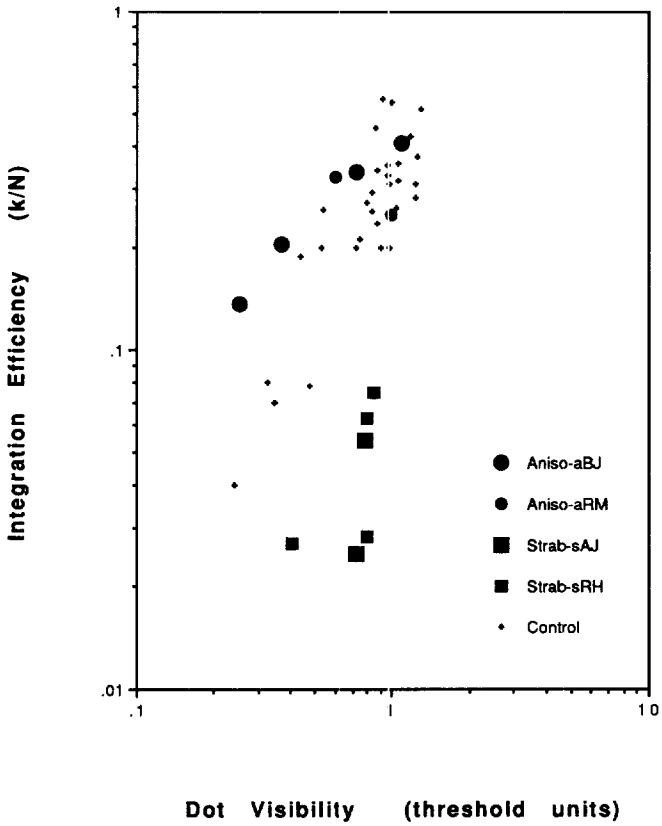

FIGURE 10. Integration efficiencies (k/N in the last column of Table 2) are plotted against dot visibility (V_d in the seventh column of Table 2) for all the observers. The same symbols are used as in Fig. 7.

are: (i) spatial uncertainty becomes less contrast dependent, but increases almost proportionally with line separation; and (ii) integration efficiency is also only reduced in strabismic eyes, but the reduction is relatively mild (less than three-fold) compared with that at the optimal line separation (more than three-fold).

DISCUSSION

In summary, our results indicate that: (i) equivalent spatial uncertainties in both anisometropic and strabismic visual systems are elevated; and (ii) equivalent integration efficiencies are reduced but only in the strabismic observers. These results not only support but also distinguish between the two hypothesized accounts (spatial uncertainty and spatial undersampling) of the spatial vision deficits in the two types of amblyopic visual systems. For the anisometropic visual system, spatial uncertainty is elevated, but spatial sampling is normal. For the strabismic visual system, both increased spatial uncertainty and spatial undersampling apply.

Relationship to previous studies

Watt and Hess (1987) estimated the intrinsic uncertainty in anisometropic amblyopes using a similar spatial perturbation paradigm. They concluded that the deficit in anisometropic spatial vision is due to an elevated spatial uncertainty, consistent with the present results. At least two alternative origins may exist for this elevated spatial uncertainty. One, as proposed by Watt and Hess (1987), is metrical scrambling, which should be relatively contrast or visibility independent. The other is a loss of contrast sensitivity in high spatial frequency filters (those related to high position sensitivity), which should be contrast sensitive. Our results (filled circles in Fig. 8) and the results in the study by Watt and Hess (1987) (additive errors in their Fig. 9 vs that in their Fig. 3) indicate that equivalent uncertainty decreases as stimulus contrast or visibility increases. Thus, the elevated spatial uncertainty in the anisometropic visual system also reflects an intensive (contrast) loss, in addition to metrical scrambling, if any. This intensive loss may, in turn, be attributed to one of two main factors. One is decreased contrast sensitivity (weak signal), and the other is increased filter size (intrinsic blur). Since any loss in contrast sensitivity has been compensated for by scaling to equal stimulus visibility (i.e., the horizontal axis in Fig. 8 is in line detection threshold units), we conclude that the size of the most sensitive filters must be enlarged (i.e., a shift in spatial scale, see Levi *et al.*, 1994c), consistent with the notion of increased intrinsic blur (Levi & Klein, 1990). Indeed, Hess and Holliday (1992) argue that the original conclusion of Watt and Hess (1987)—that anisometropic amblyopes have increased positional uncertainty—failed to take the scale shift into account (Hess and Holliday accomplished this by using band-limited patterns). In line with this, Kiorpes *et al.* (1994) reported that in amblyopic monkeys, increased positional uncertainty was accompanied by a proportional increase in intrinsic blur.

The properties of spatial sampling in the strabismic visual system have also been investigated in a previous study (Levi & Klein, 1986). The main results shown in Fig. 1 of that study indicate: (i) bisection thresholds of strabismic amblyopes were particularly elevated for stimuli consisting of a single sample compared with that of normals and anisometropic amblyopes; (ii) threshold decreased in a square root fashion as the number of samples increased; and (iii) in strabismic, but not anisometropic amblyopes, more samples were needed to reach optimal performance. These findings are basically in agreement with the present study. Since integration efficiency (k/N) decreased in the strabismic visual system (filled squares in Fig. 10), more samples (N) in the stimulus would be needed to extract a certain number of effective samples (k) required for performance to approach saturation. A decreased integration efficiency (k/N) also explains a higher bisection threshold for a fixed number of stimulus dots (N) according to the ideal averaging model [equation (1)] where the effective number of dots (k) may even become less than 1 (Table 2). The square root relationship found in the Levi and Klein (1986) study supports the ideal averaging model used in the present study.

Spatial uncertainty

Equivalent spatial uncertainty is elevated in the

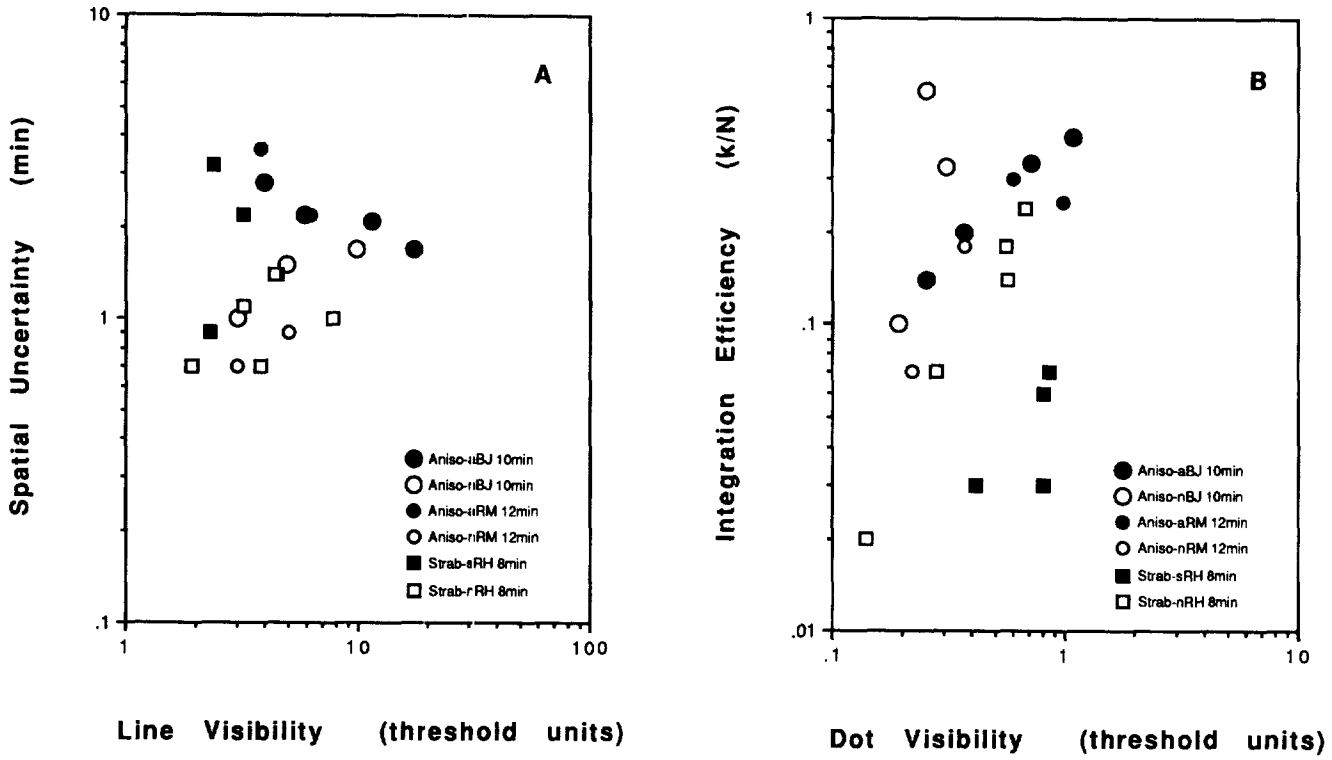

FIGURE 11. (A) Spatial uncertainty (σ_s) vs line visibility (V_l); and (B) integration efficiency (k/N) vs dot visibility (V_d) are plotted for each eye of three amblyopes tested at the same separation. Open symbols are the non-amblyopic eyes; solid symbols are the amblyopic eyes (replotted from Figs 8 and 10).

amblyopic visual systems relative to that of the normals (Fig. 8). Further, equivalent spatial uncertainties between the two types of amblyopia are comparable, implying that there is no extraordinary topographical disorder in the strabismic visual system. It is also evident in Fig. 8 that equivalent spatial uncertainty is more or less stimulus strength or visibility dependent. This is not due to any hypothesized weak signal in spatial filters, since stimulus strength has been scaled to compensate for the reduced stimulus visibility (elevated detection threshold) of the amblyopic eye. A more plausible explanation is that the size of active spatial filters may be enlarged in the amblyopic visual system (Levi *et al.*, 1994c). An enlarged filter size will also cause the effect of elevated intrinsic blur as observed previously (Levi & Klein, 1990).

There is some support for the notion that the increased spatial uncertainty in the amblyopic eyes is the consequence of the amblyopic eye using larger mechanisms. Recall that we have focused on the "optimal" separation—presumably reflecting the most sensitive mechanism. In the control and non-amblyopic eyes, the optimal separation was around 2 min. However, the optimal separation is considerably larger in the amblyopic eyes (8–12 min—see Fig. 3), presumably because the amblyopic eyes have a loss of fine resolution. In normal vision, equivalent spatial uncertainty depends on separation (Wang *et al.*, 1996), and, at small separations, visibility. Thus, a more reasonable approach may be to compare performance at the same separation in the two eyes. This comparison is shown in Fig. 11 for three of the amblyopic observers whose preferred eyes were tested at the same separations as their amblyopic eyes (8–12 min). Equivalent spatial uncertainty (σ_s) is quite similar in the two eyes of each observer when tested at the same separation [Fig. 11(A)], particularly at the higher visibility levels. Therefore, we conclude that the apparent increase in σ_s in the amblyopic eyes is largely a consequence of an increase in the size of the most sensitive filter (relative to that of the preferred eye), i.e., a shift in the spatial scale of analysis in the amblyopic eye to larger mechanisms (Levi *et al.*, 1994c).

An increase in the size of active filters could be a direct consequence of abnormal development in amblyopic visual systems. In the case of anisometropic amblyopia, the retinal image is blurred in the amblyopic eye, which compromises the development of small sized filters tuned to fine details. This drop-out of the functionality of small sized filters leads to an increase in the effective size of active filters. In the case of strabismic amblyopia, the mismatched retinal images in the two eyes results in the image from the strabismic eye being suppressed at a stage where the images from the two eyes converge. This inhibition probably plays a detrimental role in the development of function in the strabismic cortex, where the small sized filters may be highly vulnerable.

Spatial undersampling

Equivalent integration efficiency is decreased, but only in the strabismic visual system (Fig. 10). The loss of

spatial integration efficiency implies an inability to use information from discrete samples in the strabismic visual system. There are at least two alternative stages in the strabismic visual pathway where this loss may take place. One is at an early stage (where the samples are detected), and the other is at a higher stage (where the sample integration takes place). The loss of spatial integration persists even for equally well detected or visible dots (Fig. 10), indicating that spatial undersampling for spatial position judgments must take place beyond the early detection stage, at a secondary (higher) stage of the strabismic visual pathway. The loss of spatial integration efficiency (k/N) of strabismic amblyopes also persists when performance of the two eyes is compared at the same separation [Fig. 11(B)]. In this figure it is evident that compared with the preferred eye at the same separation, strabismic amblyope RH has a very marked reduction in spatial integration efficiency. Thus, spatial undersampling may be understood in terms of efficiency loss in utilizing detected spatial information. Such spatial undersampling is a reasonable consequence of abnormal development in the strabismic visual system, where the "misaligned" spatial information from the strabismic eye must be suppressed at a higher binocular integration stage of the visual pathway. Perhaps the "undersampling" evident in our strabismic amblyopes might be thought of as a form of visual "neglect".

The notion of undersampling is highly contentious (see Levi & Klein, 1996; Hess & Field, 1994). For example, Hess and Field (1994) argue that undersampling should have a predictable effect on contrast and position judgments. However, a model incorporating undersampling and large univariant mechanisms (Levi & Klein, 1996) can readily account for the decoupling of contrast and position reported by Hess and Field. Moreover, if position discrimination is processed at a later stage than contrast discrimination, then undersampling at the second stage would only affect the position judgment, since the contrast information was being used from the first stage.

While there is strong evidence for spatial undersampling in the normal periphery (Coletta & Williams, 1987; Coletta, Williams & Tiana, 1990; Anderson & Hess, 1990) based on the perception of reversed motion, to date there have been only tantalizing hints of undersampling in amblyopes. For example, Hess, Campbell and Greenhalgh (1978) and more recently Bradley and Thibos (1988) have reported that for some amblyopes, grating patterns appear distorted, and these distortions look strikingly similar to the "zebra stripes" described by Williams (1985), and ascribed to aliasing. However, these reports are subjective, and there may be other plausible explanations for the distorted appearance of the gratings (some of the pictures look like near threshold gratings in normal vision). One direct line of evidence for undersampling in amblyopia would be the perception of motion reversal or orientation reversal, when viewing with the amblyopic fovea. Hess and Anderson (1993) argue against undersampling, because they were not able to demonstrate motion reversal in their small group of amblyopic subjects using directly viewed gratings. The failure to observe motion reversal does not necessarily imply that undersampling does not occur (Wang, Thibos & Bradley, 1995; Artal, Derrington & Colombo, 1995). Recent experiments, using coherent light, have demonstrated large errors in perceived orientation in the central field of strabismic amblyopes (including one of the two observers in our study) at spatial frequencies much lower than the cone Nqyuist limit. The inability to make veridical orientation matches is consistent with undersampling at a post-receptoral stage (Sharma, Levi & Coletta, 1997). The dramatic loss of cortical neurons driven through the amblyopic eye (Wiesel, 1982; Baker, Grigg & von Noorden, 1974) could provide a neural substrate for undersampling.

CONCLUSION

Spatial uncertainty is elevated in both anisometropic and strabismic visual systems by approx. ten-fold. This increase in spatial uncertainty may be mainly due to the loss of functionality in small sized spatial filters, thus the average size of active spatial filters is enlarged. Spatial undersampling is only found in the strabismic visual systems in terms of a loss in spatial integration efficiency. We speculate that spatial undersampling takes place at a secondary stage in the visual pathway beyond the early detection stage. Both deficits of elevated spatial uncertainty and spatial undersampling can be related to the developmental disorders in the amblyopic visual systems.

REFERENCES

Anderson, S. J. & Hess, R. F. (1990). Post-receptoral undersampling in normal human peripheral vision. *Vision Research, 30*, 1507–1516.

Andrews, D. P., Butcher, A. K. & Buckley, B. R. (1973). Acuities for spatial arrangement in line figures: human and ideal observers compared. *Vision Research, 13*, 599–620.

Artal, P., Derrington, A. M. & Colombo, E. (1995). Refraction, aliasing, and the absence of motion reversals in peripheral vision. *Vision Research, 35*, 939–947.

Baker, F. H., Grigg, P. & von Noorden, G. K. (1974). Effects of visual deprivation and strabismus on the responses of neurons in the visual cortex of the monkey, including studies on the striate and prestriate cortex in the normal animal. *Brain Research, 66*, 185–208.

Barlow, H. B. (1962). A method for determining the overall quantum efficiency of visual discriminations. *Journal of Physiology, London, 160*, 155–168.

Bradley, A. & Thibos, L. N. (1988). Perceptual aliasing in human amblyopia. *Investigative Ophthalmology & Visual Science, 29 Suppl.*, 76.

Coletta, N. J. & Williams, D. R. (1987). Psychophysical estimate of extrafoveal cone spacing. *Journal of the Optical Society of America A, 4*, 1503–1513.

Coletta, N. J., Williams, D. R. & Tiana, C. L. M. (1990). Consequences of spatial sampling for human motion perception. *Vision Research, 30*, 1631–1648.

Hess, R. F. & Anderson, S. J. (1993). Motion sensitivity and spatial undersampling in amblyopia. *Vision Research, 33*, 881–896.

Hess, R. F., Campbell, F. W. & Greenhalgh, T. (1978). On the nature of the neural abnormality in human amblyopia: neural aberrations and neural sensitivity loss. *Pflugers Archives, 377*, 201–207.

Hess, R. F. & Field, D. (1994). Is the spatial deficit in strabismic amblyopia due to loss of cells or an uncalibrated disarray of cells? *Vision Research, 34*, 3397–3406.

Hess, R. F., Field, D. & Watt, R. J. (1990). The puzzle of amblyopia. In C. Blakemore (Ed.), *Vision: coding and efficiency*. Cambridge, U.K.: Cambridge University Press.

Hess, R. F. & Holliday, I. E. (1992). The spatial localization deficit in amblyopia. *Vision Research, 32*, 1319–1339.

Kiorpes, L., Kiper, D. C. & Movshon, J. A. (1994). The effect of blur and positional jitter on Vernier acuity in normal and amblyopic macaque monkeys. *Investigative Ophthalmology & Visual Science, 35 Suppl*, 2064.

Klein, S. A., Casson, E. & Carney, T. (1990). Vernier acuity as line and dipole detection. *Vision Research, 30*, 1703–1719.

Levi, D. M. (1991). Spatial vision in amblyopia. In D. Regan (Ed.), *Spatial vision* (pp. 212–238). London: MacMillan Press.

Levi, D. M. & Klein, S. A. (1985). Vernier acuity, crowding and amblyopia. *Vision Research, 25*, 979–991.

Levi, D. M. & Klein, S. A. (1986). Sampling in spatial vision. *Nature, 320*, 360–362.

Levi, D. M. & Klein, S. A. (1990). Equivalent intrinsic blur in amblyopia. *Vision Research, 30*, 1995–2022.

Levi, D. M. & Klein, S. A. (1996). Limitations on position coding imposed by undersampling and univariance. *Vision Research, 36*, 2111–2120.

Levi, D. M., Klein, S. A. & Aitsebaomo, A. P. (1984). Detection and discrimination of the direction of motion in central and peripheral vision of normal and amblyopic observers. *Vision Research, 24*, 789–800.

Levi, D. M., Klein, S. A. & Wang, H. (1994a) Amblyopic and peripheral Vernier acuity: a test-pedestal approach. *Vision Research, 34*, 3265–3292.

Levi, D. M., Klein, S. A. & Wang, H. (1994b) Discrimination of position and contrast in amblyopic and peripheral vision. *Vision Research, 34*, 3293–3314.

Levi, D. M., Klein, S. A. & Yap, Y. L. (1987). Positional uncertainty in peripheral and amblyopic vision. *Vision Research, 27*, 581–597.

Levi, D. M., Waugh, S. J. & Beard, B. L. (1994c) Spatial scale shifts in amblyopia. *Vision Research, 34*, 3315–3334.

Morgan, M. J. & Glennerster, A. (1991). Efficiency of locating centers of dot-clusters by human observers. *Vision Research, 31*, 2075–2083.

Pelli, D. G. (1990). The quantum efficiency of vision. In C. Blakemore (Ed.), *Vision: coding and efficiency*. Cambridge, U.K.: Cambridge University Press.

Sharma, V, Levi, D. M. & Coletta, N. J. (1997). Sparse sampling in central vision of strabismic amblyopes. *Investigative Ophthalmology and Visual Science* (Suppl.) *38*, S108.

Wang, H., Levi, D. M. & Klein, S. A. (1996). Intrinsic uncertainty and integration efficiency in bisection acuity. *Vision Research, 36*, 717–739.

Wang, Y. Z., Thibos, L. N. & Bradley, A. (1995). Motion perception of aliased gratings in the periphery, *Investigative Ophthalmology & Visual Science*, (Suppl. 36), S55.

Watt, R. J. & Andrews, D. P. (1982). Contour curvature analysis: hyperacuities in the discrimination of detailed shape. *Vision Research, 22*, 449–460.

Watt, R. J. & Hess, R. F. (1987). Spatial information and uncertainty in anisometropic amblyopia. *Vision Research, 27*, 661–674.

Watt, R. J., Ward, R. & Casco, C. (1987). The detection of deviation from straightness in lines. *Vision Research, 27*, 1659–1678.

Wiesel, T. N. (1982). Postnatal development of the visual cortex and the influence of environment. *Nature, 299*, 583–591.

Williams, D. R. (1985). Aliasing in human foveal vision. *Vision Research, 25*, 195–205.

Wilson, H. R. (1991). Pattern discrimination, visual filter, and spatial sampling irregularity. In M. S. Landy & J. A. Movshon (Eds), *Computational models of visual processing* (pp. 153–168). Cambridge. MA: The MIT Press.

Zeevi, Y. Y. & Mangoubi, S. S. (1984). Vernier acuity with noisy lines: estimation of relative position uncertainty. *Biological Cybernetics, 50*, 371–376.

Acknowledgements—This study was supported by NIH Grants F32 EY06601, RO1 EY01728, and RO1 EY04776. We thank Robert Hess and an anonymous referee for their helpful comments on an earlier draft.